NANOPARTICLE SHAPE EFFECT ON THE NATURAL-CONVECTION HEAT TRANSFER OF HYBRID NANOFLUID INSIDE A U-SHAPED ENCLOSURE

by

Muhammad Solleh ASMADI[a], Zailan SIRI[a*], Ruhaila Md. KASMANI[b], and Habibis SALEH[c]

[a] Institute of Mathematical Sciences, Faculty of Science,
Universiti Malaya, Kuala Lumpur, Malaysia
[b] Mathematics Division, Centre for Foundation Studies in Science,
Universiti Malaya, Kuala Lumpur, Malaysia
[c] Mathematics Education Department,
Universitas Islam Negeri Sultan Syarif Kasim, Pekanbaru, Indonesia

Original scientific paper
https://doi.org/10.2298/TSCI200818139A

The effect of nanoparticle shape on the natural-convection heat transfer of Cu-Al_2O_3-water hybrid nanofluid inside a U-shaped enclosure is presented in this paper. The governing equations are transformed into the dimensionless form using dimensionless variables. A three-node triangular finite element method is used with the Newton-Raphson method to solve the problem numerically. The streamlines and isotherms as well as the local and average Nusselt numbers are presented for the fluid-flow with Rayleigh number of 10^4 to 10^6. It is found that blade nanoparticle shape produces the highest heat transfer rate while sphere is the lowest.

Key words*: natural-convection, hybrid nanofluid, nanoparticle shape, U-shaped enclosure, heat transfer*

Introduction

Heat transfer through natural-convection in an enclosure has been an ongoing research topic worldwide especially in engineering and industrial applications. Some of the examples are the cooling system inside smartphones and nuclear reactors. Lately, the study of natural-convection heat transfer has been directed towards the usage of nanofluids. Nanoparticles such as Cu and Al_2O_3 are suspended in the base fluids such as water or oil which enhances the heat transfer due to the high thermal conductivity of the nanoparticle. The exploration of nanofluid in a *U*-shaped or *C*-shaped cavity has been done by Cho *et al.* [1], Ghasemi [2], Mohebbi [3], and Ma *et al.* [4], which show a great improvement in the thermal enhancement of nanofluid compared to pure water. Ali *et al.* [5], Kilic and Ali [6] investigate the application of nanofluids in car radiator and impinging jets, respectively.

Metallic nanoparticles have a relatively high thermal conductivity and reactivity with the base fluids. It is expensive to produce. In contrast, metallic oxides nanoparticles have a relatively low thermal conductivity, more stable and cheaper than metallic particles [7]. By exploiting the positive characteristics of both nanoparticles, a hybrid nanofluid is explored by mixing a metallic and metallic oxide nanoparticles dispersed in a common base fluid. The ad-

* Corresponding author, e-mail: zailansiri@um.edu.my

vantage of the positive enhancement in both nanoparticles can be taken without loses the other. For example, Cu-Al_2O_3-water hybrid nanofluid has a relatively high thermal conductivity, low reactivity and can be procured at a lower cost. Investigation of natural-convection of hybrid nanofluid is extensively studied by Hayat and Nadeem [8], Tayebi and Oztop [9], Tayebi *et al.* [10], Al-Srayyih *et al.* [11], and Tayebi and Chamkha [12].

Based on the literature review, there is a very little investigation done on the natural-convection inside a *U*-shaped enclosure with a single heating source (bottom wall) with varying nanoparticle shape. Most of the study focused on three heating sources located on the left, bottom and right wall. This paper aimed to explore the effect of hybrid nanoparticle shape on the heat transfer of Cu-Al_2O_3-water hybrid nanofluid inside a *U*-shaped enclosure. The governing equations are transformed into a dimensionless equation by using dimensionless variables. The problem is solved numerically by employing a robust three-node triangular finite element method (FEM) with Newton-Rahpson iterative method. The effect of nanoparticle shape and the size of the cold rib are studied by varying selected parameters. The heat transfer rate is presented in the form of the local and averaged Nusselt number.

Mathematical formulations

The schematic diagram of the enclosure is presented in fig. 1(a). The enclosure is a square with the length and height of W, and the cold rib EFGJ has the length of L_C and height of H_C, with $L_C = H_C$. The bottom wall BC is heated with a constant temperature T_H and the cold rib EFGJ is cooled with a constant temperature T_C, where $T_H > T_C$. The walls AB, CD, DE, and JA are thermally insulated. The velocity direction of u and v are in the direction of x- and y-axis, respectively, with the gravity force is in the direction of the negative y-axis. The enclosure is filled with Cu-Al_2O_3-water hybrid nanofluid. By employing Boussinesq approximation, the dimensionless governing equations of the aforementioned system are:

$$\frac{\partial U}{\partial X}+\frac{\partial V}{\partial Y}=0 \tag{1}$$

$$U\frac{\partial U}{\partial X}+V\frac{\partial U}{\partial Y}=-\frac{\partial P}{\partial X}+\frac{\mu_{\mathrm{hnf}}}{\rho_{\mathrm{hnf}}\alpha_{\mathrm{bf}}}\left(\frac{\partial^2 U}{\partial X^2}+\frac{\partial^2 U}{\partial Y^2}\right) \tag{2}$$

$$U\frac{\partial V}{\partial X}+V\frac{\partial V}{\partial Y}=-\frac{\partial P}{\partial Y}+\frac{\mu_{\mathrm{hnf}}}{\rho_{\mathrm{hnf}}\alpha_{\mathrm{bf}}}\left(\frac{\partial^2 V}{\partial X^2}+\frac{\partial^2 V}{\partial Y^2}\right)+\mathrm{RaPr}\theta\frac{(\rho\beta)_{\mathrm{hnf}}}{\rho_{\mathrm{hnf}}\beta_{\mathrm{bf}}} \tag{3}$$

$$U\frac{\partial \theta}{\partial X}+V\frac{\partial \theta}{\partial Y}=\frac{\alpha_{\mathrm{hnf}}}{\alpha_{\mathrm{bf}}}\left(\frac{\partial^2 \theta}{\partial X^2}+\frac{\partial^2 \theta}{\partial Y^2}\right) \tag{4}$$

where $\mathrm{Pr} = \nu_{\mathrm{bf}}/\alpha_{\mathrm{bf}}$ and $\mathrm{Ra} = [g\beta_{\mathrm{bf}}W^3(T_H - T_C)]/\alpha_{\mathrm{bf}}\nu_{\mathrm{bf}}$ are the Prandtl and Rayleigh numbers, respectively. The subscripts hnf, bf, hp, Cu, and Al_2O_3 correspond to the hybrid nanofluid, base fluid, hybrid nanoparticles, copper, and alumina, respectively. Equations (1)-(4) are transformed using dimensionless variables:

$$X=\frac{x}{W},\ Y=\frac{y}{W},\ U=\frac{uW}{\alpha_{\mathrm{bf}}},\ V=\frac{vW}{\alpha_{\mathrm{bf}}},\ P=\frac{pW^2}{\rho_{\mathrm{bf}}\alpha_{\mathrm{bf}}^2},\ \theta=\frac{T-T_C}{T_H-T_C} \tag{5}$$

where T, $\alpha = k/\rho C_p$, ρ, C_p, β, μ, and ν are temperature, thermal diffusivity, density, heat capacity, thermal expansion coefficient, dynamic viscosity, and kinematic viscosity of the fluid or

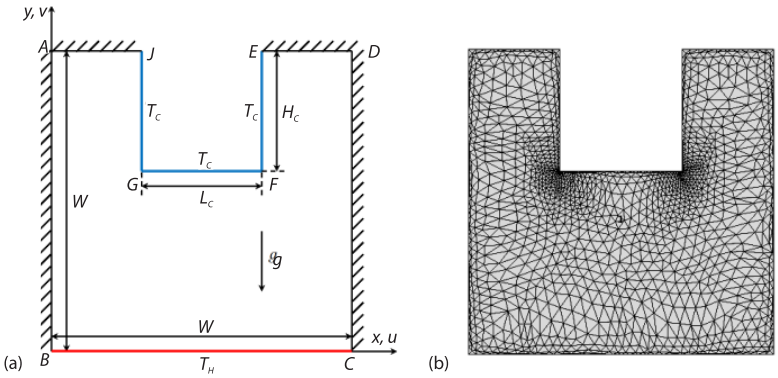

Figure 1. Schematic diagram of: (a) the enclosure and (b) a triangular meshing of the enclosure

nanoparticle, respectively. The thermophysical properties of the base fluid and nanoparticles are shown in tab. 1. The dimensionless velocity boundary conditions to the enclosure as shown in fig. 1(a) are:

$$\begin{aligned} &\text{at all surface}: U = V = 0 \\ &\text{at AB, CD, EF and GJ}: \frac{\partial U}{\partial Y} = 0 \\ &\text{at BC, DE, FG and JA}: \frac{\partial V}{\partial X} = 0 \end{aligned} \tag{6}$$

Table 1. Thermophysical properties of the materials used in this study [13]

Materials	Water	Cu	Al_2O_3
Specific heat capacity, C_p [Jkg^{-1}K^{-1}]	4179	385	765
Density, ρ [kgm^{-3}]	997.1	8933	3970
Thermal conductivity, k [Wm^{-1}K^{-1}]	0.613	401	40
Thermal expansion coefficient, β [K^{-1}]	21	$1.67 \cdot 10^{-5}$	$0.85 \cdot 10^{-5}$

The dimensionless temperature boundary conditions to the enclosure as shown in fig. 1(a) are:

$$\begin{aligned} &\text{at BC}: \theta = 1 \\ &\text{at EF, FG and GJ}: \theta = 0 \\ &\text{at AB and CD}: \frac{\partial \theta}{\partial X} = 0 \\ &\text{at DE and JA}: \frac{\partial \theta}{\partial Y} = 0 \end{aligned} \tag{7}$$

The dimensionless stream function, Ψ, is defined where $U = \partial\Psi/\partial Y$ and $V = -\partial\Psi/\partial X$. The hybrid nanoparticle volume fraction, ϕ_{hp}, hybrid density, ρ_{hp}, hybrid thermal expansion coefficient, β_{hp}, hybrid thermal conductivity, k_{hp}, and hybrid heat capacity, $(C_p)_{hp}$ respectively, are [12]:

$$\phi_{hp} = \phi_{Cu} + \phi_{Al_2O_3} \tag{8}$$

$$\rho_{\mathrm{hp}} = \frac{\phi_{\mathrm{Cu}}\rho_{\mathrm{Cu}} + \phi_{\mathrm{Al_2O_3}}\rho_{\mathrm{Al_2O_3}}}{\phi_{\mathrm{hp}}} \tag{9}$$

$$\beta_{\mathrm{hp}} = \frac{\phi_{\mathrm{Cu}}\beta_{\mathrm{Cu}} + \phi_{\mathrm{Al_2O_3}}\beta_{\mathrm{Al_2O_3}}}{\phi_{\mathrm{hp}}} \tag{10}$$

$$k_{\mathrm{hp}} = \frac{\phi_{\mathrm{Cu}}k_{\mathrm{Cu}} + \phi_{\mathrm{Al_2O_3}}k_{\mathrm{Al_2O_3}}}{\phi_{\mathrm{hp}}} \tag{11}$$

$$\left(C_p\right)_{\mathrm{hp}} = \frac{\phi_{\mathrm{Cu}}\left(C_p\right)_{\mathrm{Cu}} + \phi_{\mathrm{Al_2O_3}}\left(C_p\right)_{\mathrm{Al_2O_3}}}{\phi_{\mathrm{hp}}} \tag{12}$$

The effective density, ρ_{hnf}, effective specific heat capacity $(\rho C_p)_{\mathrm{hnf}}$, effective thermal diffusivity α_{hnf}, and effective thermal expansion coefficient β_{hnf}, respectively are [12]:

$$\rho_{\mathrm{hnf}} = \left(1-\phi_{\mathrm{hp}}\right)\rho_{\mathrm{bf}} + \phi_{\mathrm{hp}}\rho_{\mathrm{hp}} \tag{13}$$

$$\left(\rho C_p\right)_{\mathrm{hnf}} = \left(1-\phi_{\mathrm{hp}}\right)\left(\rho C_p\right)_{\mathrm{bf}} + \phi_{\mathrm{hp}}\left(\rho C_p\right)_{\mathrm{hp}} \tag{14}$$

$$\beta_{\mathrm{hnf}} = \left(1-\phi_{\mathrm{hp}}\right)\beta_{\mathrm{bf}} + \phi_{\mathrm{hp}}\beta_{\mathrm{hp}} \tag{15}$$

$$\alpha_{\mathrm{hnf}} = \frac{k_{\mathrm{hnf}}}{\left(\rho C_p\right)_{\mathrm{hnf}}} \tag{16}$$

The effective dynamic viscosity, μ_{hnf}, given by Brinkman [14] is used due to the simplicity and acceptable to use as a general governing behavior of nanoparticles. The μ_{hnf} is given:

$$\mu_{\mathrm{hnf}} = \frac{\mu_{\mathrm{bf}}}{\left(1-\phi_{\mathrm{hp}}\right)^{2.5}} \tag{17}$$

The thermal conductivity of the hybrid nanofluid given by Hamilton and Crosser [15] is given:

$$\frac{k_{\mathrm{hnf}}}{k_{\mathrm{bf}}} = \frac{k_{\mathrm{hp}} + \left(m-1\right)k_{\mathrm{bf}} - \left(m-1\right)\phi_{\mathrm{hp}}\left(k_{\mathrm{bf}} - k_{\mathrm{hp}}\right)}{k_{\mathrm{hp}} + \left(m-1\right)k_{\mathrm{bf}} + \phi_{\mathrm{hp}}\left(k_{bf} - k_{\mathrm{hp}}\right)} \tag{18}$$

where m is the nanoparticle shape factor as listed in tab. 2. In this study, the nanoparticle shape for both Cu and Al_2O_3 are equivalent.

The rate of heat transfer in the enclosure is measured using local and averaged Nusselt number. The rate of heat transfer at a local position relative to the wall is denoted as $\mathrm{Nu_{loc}}$, where [9-12]:

$$\mathrm{Nu_{loc}} = -\frac{k_{\mathrm{hnf}}}{k_{\mathrm{bf}}}\frac{\partial\theta}{\partial Y} \tag{19}$$

The averaged rate of heat transfer, $\overline{\mathrm{Nu}}$ along the hot wall BC:

$$\overline{\mathrm{Nu}} = \int_0^1 \mathrm{Nu_{loc}}\,\mathrm{d}X \tag{20}$$

Table 2. Nanoparticle empirical shape factor [16]

Shape	Shape factor, m
Sphere	3
Cube/brick	3.7
Cylindrical	4.9
Platelet/discoid	5.7
Blade/oblate spheroid	8.6

Method of solution

The governing equations in eqs. (1)-(4) are numerically solved by employing the three-node triangular FEM [17]. The enclosure is discretised into a triangular mesh of a certain number of elements.

An example of the meshing is shown in fig. 1(b). The Galerkin weighted residual FEM is chosen to solve the problem. Each node of the triangular element in the enclosure is assigned with a value corresponding to their velocity, temperature and pressure at the nodes according to the boundary conditions in eqs. (6) and (7). The values assigned are then coupled and compiled into a matrix and is solved using LU decomposition algorithm. The solutions are then iterated using damped Newton-Raphson non-linear iteration method [18] until the residuals are within the tolerance level of $\varepsilon = 10^{-3}$.

Mesh dependency test is carried out to ensure the independence of the results to the mesh sizes. Table 3 shows the mesh configurations along with their resulting averaged Nusselt number, and maximum stream function value, $|\Psi_{max}|$ with $H_C = L_C = 0.4$, $m = 3$, and $Ra = 10^5$. The percentage errors are calculated using:

$$\text{Error}_{new} = \frac{\left|\chi_{new} - \chi_{old}\right|}{\chi_{old}} \times 100\% \tag{21}$$

where χ is $\overline{Nu}$ or $|\Psi_{max}|$. Based on tab. 3, meshing VIII are chosen because the percentage error for meshing IX are within 0.1%. This is to ensure that the results are within tolerance level without compensating the computational time.

Table 3. The value of $\overline{Nu}$, $|\Psi_{max}|$ and corresponding error [%] for different type of meshing

Meshing type	Number of triangular elements	$\overline{Nu}$		$\lvert\Psi_{max}\rvert$	
		Value	Error [%]	Value	Error [%]
I	360	5.7785	0.000000	6.1170	0.000000
II	606	5.7600	0.321181	6.3624	3.856261
III	870	5.7438	0.282043	6.5877	3.419581
IV	1590	5.7314	0.216352	6.7962	3.069197
V	2280	5.7199	0.201052	6.8927	1.398879
VI	3430	5.7091	0.189172	6.9432	0.727478
VII	9034	5.7012	0.138567	6.9909	0.682461
VIII	23674	5.6964	0.084264	7.0233	0.461465
IX	28864	5.6950	0.024583	7.0290	0.081093

Table 4 shows the comparison of averaged Nusselt number, for different Rayleigh number between [19] and present work for CuO-water nanofluid with $H_C = L_C = 0.4$ and $m = 3$, and hot wall at AB, BC, and CD at an inclination of 90 °C (*C*-shaped enclosure configuration). Good agreement between the results is observed, as indicated in tab. 4, with percentage error is less than 3%. Thus, our numerical code and mathematical calculations are indeed verified.

Table 4. Comparison of $\overline{Nu}$ from [19] with the present results

Ra	[19]	Present	Error [%]
10^3	1.834	1.8133	1.129
10^4	1.883	1.8352	2.539
10^5	2.611	2.6058	0.1992
10^6	4.733	4.7380	0.1056

Results and discussion

In this study, the ratio of the nanoparticle volume fraction is fixed at $\phi_{Cu}:\phi_{Al2O3} = 1:1$ unless stated otherwise. The values of $\overline{Nu}$ for several nanoparticle volume fractions ϕ_{hp} are plotted with different Rayleigh number with $H_C = L_C = 0$ and $m = 3$ in fig. 2(a). From fig. 2(a), the values of $\overline{Nu}$ increase with an increase in ϕ_{hp} for $10^4 \leq Ra \leq 10^6$. The values of $\overline{Nu}$ increase significantly as ϕ_{hp} increases. That means the addition of hybrid nanoparticles to the base fluid of higher Rayleigh number value greatly helps the heat transfer inside the enclosure than the base fluid with lower Rayleigh number value. Figure 2(b) shows the variations of the $\overline{Nu}$ at the hot wall against the nanoparticle volume fraction for different types of nanofluid with $H_C = L_C = 0.4$, $m = 3$, and $Ra = 10^5$. Based on fig. 2(b), the values of $\overline{Nu}$ for Cu-Al_2O_3-water hybrid nanofluid are higher than Cu-water and Al_2O_3-water nanofluids for $0 \leq \phi_{hp} \leq 0.08$. For $\phi_{hp} = 0.1$, the values of $\overline{Nu}$ for Cu-water nanofluid are higher than Cu-Al_2O_3-water and Al_2O_3-water nanofluids. Based on the literature survey, the value of $\overline{Nu}$ is expected to be $\overline{Nu}_{Cu} \leq \overline{Nu}_{hybrid} \leq \overline{Nu}_{Al2O3}$ for all ϕ_{hp}. The unusual behavior of $\overline{Nu}$ for lower ϕ_{hp} is suspected due to the shape of the enclosure, the heating and cooling position and the aspect ratio of the cold rib EFGJ. This shows that addition of Cu nanoparticles to Al_2O_3-water nanofluid increases heat transfer.

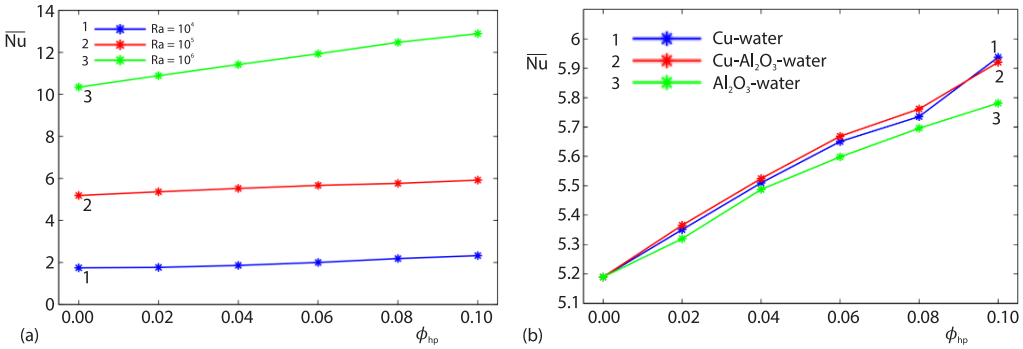

Figure 2. The variation of average Nusselt numbers at the hot wall for different nanoparticle volume fractions with (a) different Rayleigh numbers and (b) different type of nanofluids and hybrid nanofluid with $H_C = L_C = 0.4$, $m = 3$, and $Ra = 10^5$

The high thermal conductivity of Cu nanoparticles helps the heat dissipation of Al_2O_3-water nanofluid without losing the low reactivity of Al_2O_3 with a fraction of cost.

Figure 3 presents the effect of nanoparticle volume fraction ratios to the $\overline{Nu}$ with $\phi_{hp} = 0.1$, $H_C = L_C = 0.4$, $m = 3$, and Ra = 10^5. It is found that by replacing 25% of Al_2O_3 by volume with Cu nanoparticles (indicated by the ratio of $\phi_{Cu} : \phi_{Al_2O_3} = 0.025 : 0.075$, the values of $\overline{Nu}$ increase significantly. Subsequent nanoparticle replacing does increase the value of $\overline{Nu}$ but not as significant as the first 25%. That means the hybrid nanofluid of Cu-Al_2O_3-water is better in terms of heat transfer than Al_2O_3-water with the same value of ϕ_{hp}. Replacing a small volume of Al_2O_3 with Cu nanoparticles is the best configuration enhance heat transfer due to its significant increase of $\overline{Nu}$ while keeping the cost down.

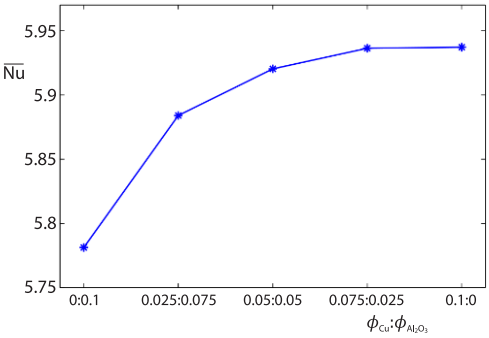

Figure 3. The effect of different nanoparticle volume fraction ratios of Cu and Al_2O_3 to the $\overline{Nu}$ with $H_C = L_C = 0.4$, $m = 3$, and Ra = 105

Figure 4 shows the effects of Rayleigh number and the dimension of the cold rib to the streamlines of the fluid-flow inside the enclosure for $m = 3$ and $\phi_{hp} = 0.05$. Based on fig. 4, all configuration of Rayleigh numbers $10^4 \leq Ra \leq 10^6$ and cold rib dimension $0.2 \leq L_C = H_C \leq 0.6$ produce two symmetric Rayleigh-Benard cells. The presence of the symmetric cold rib forces

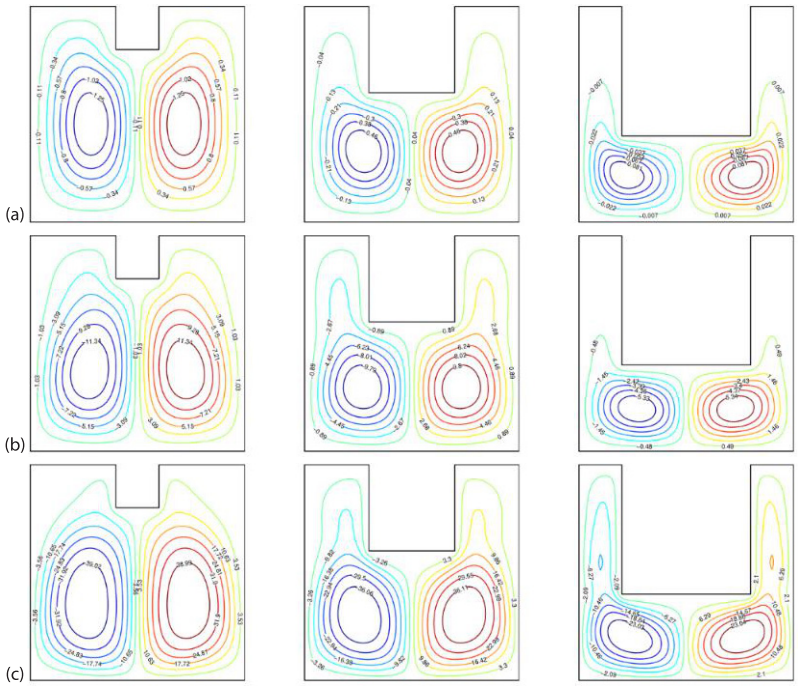

Figure 4. The effects of Rayleigh number and the dimension of the cold rib to the streamlines with $m = 3$ and $\phi_{hp} = 0.05$; (a) $L_C = H_C = 0.2$ and Ra = 10^4, (b) $L_C = H_C = 0.4$ and Ra = 10^5, and (c) $L_C = H_C = 0.6$ and Ra = 10^6

the fluid-flow to separate into two identical cells with opposing direction. It can be seen that for a constant Rayleigh number, the size of cells decreases as the cold rib dimension increases. This is due to the decreasing space available for the fluid to flow inside the enclosure. As the cold rib dimension increases, the streamlines become closer to each other, especially at the vicinity of the cold rib corner F and G. The longer cold rib side causes the fluid to be contained in a narrow space before being released at the bottom part of the enclosure. This produces a higher fluid velocity at the area of the corner F and G. It is also noted that as the cold rib dimension increases, streamlines do not reach the area to the left and right of the cold rib for $10^4 \leq \mathrm{Ra} \leq 10^5$, but not for $\mathrm{Ra} = 10^6$. This is due to the increase of the buoyancy force as Rayleigh number increases, which is enough to overcome the gravity force. Thus the fluid is able to flow towards the upper part of the enclosure. For a constant cold rib dimension, the streamlines are closer to the side wall as Rayleigh number increases. The higher buoyancy force presents in the enclosure produced a higher fluid velocity near to the side wall of the enclosure. This is due to the fluid-flow becoming more turbulent than laminar flow at the lower Rayleigh number. It is also noted that the maximum stream function value $|\Psi_{\max}|$ increases as Rayleigh number increases, but decreases as the cold rib dimension increases.

Figure 5 shows the effects of Rayleigh number and the dimension of the cold rib to the isotherms of the fluid-flow inside the enclosure for $m = 3$ and $\phi_{\mathrm{hp}} = 0.05$. For a constant cold rib dimension, the isotherm lines are about parallel for $\mathrm{Ra} = 10^4$, but becoming more turbulent as Rayleigh number increases. This behaviour is due to the increasing heat convection mechanism as Rayleigh number increases. Heat convection becomes more dominant than heat conduction at higher Rayleigh number due to the turbulent flow produced by higher buoyancy

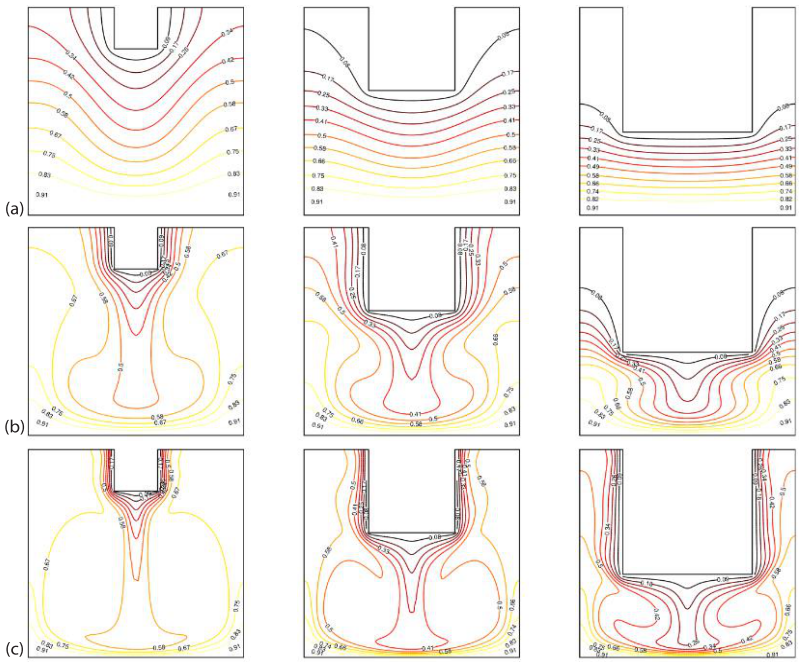

Figure 5. The effect of Rayleigh number and the dimension of the cold rib to the isotherms with $m = 3$ and $\phi_{\mathrm{hp}} = 0.05$; (a) $L_{\mathrm{C}} = H_{\mathrm{C}} = 0.2$ and $\mathrm{Ra} = 10^4$, (b) $L_{\mathrm{C}} = H_{\mathrm{C}} = 0.4$ and $\mathrm{Ra} = 10^5$, and (c) $L_{\mathrm{C}} = H_{\mathrm{C}} = 0.6$ and $\mathrm{Ra} = 10^6$

force in the enclosure. As Rayleigh number increases, the isotherm lines pattern follows more the corresponding streamlines pattern. As a result, the heat transfer of the fluid increases. At Ra = 10^4, the isotherm lines are about parallel and follow the shape of the cold rib for lower cold rib dimension, but they became parallel to the hot wall as Rayleigh number increases. This phenomenon occurs because the width of the cold rib becomes longer and the cold rib is closer to the side walls of the enclosure, producing narrower area at the top of the enclosure. At lower Rayleigh number, buoyancy forces are not strong enough to help heat transfer to undergo heat convection and dissipate through the narrow passage. For a constant Rayleigh number, the isotherm lines are closer to each other due to less enclosure space and less distance between the hot and the cold wall. For Ra = 10^5, the isotherm lines are very close to the vicinity of the cold rib corners F and G. This is because the fluid has to flow through the narrower area at the top of the enclosure before being rushed to the wider area at the bottom of the enclosure. This makes the heat transfer of the fluid at the highest rate near the cold rib corners F and G for Ra $\geq 10^5$.

Figure 6 presents the velocity vectors with velocity magnitude and isosurface with m = 3, $H_C = L_C = 0.4$, Ra = 10^5 and $\phi_{hp} = 0.05$. In fig. 7(a), the red area denotes higher fluid velocity and the blue area denotes lower fluid velocity. It can be seen from fig. 6(a) that the fluid velocity is at the highest around the middle area of the enclosure directly below the cold rib. The fluid-flow from the two symmetric cells merges at the middle area and produces a greater velocity than the rest of the enclosure.

In fig. 6(b), the hottest fluid is colored white and the coldest fluid is colored red. It can be seen that the buoyancy force brings the hot fluid towards the top of the enclosure and the cold fluid down. It is noteworthy to mention that the less dense hot fluid tends to move upwards by buoyancy force and the denser cold fluid tends to move downwards following gravity force. This fluid movement produces the isosurface pattern from fig. 6(b). Hot fluid moves upwards along the side walls while cold fluid moves downwards at the middle of the enclosure. Reason for this is that the cold rib is closer to the hot wall in the middle, and the fact that the enclosure is symmetric at the middle of the enclosure, results in the cold fluid to move in one flow in the middle.

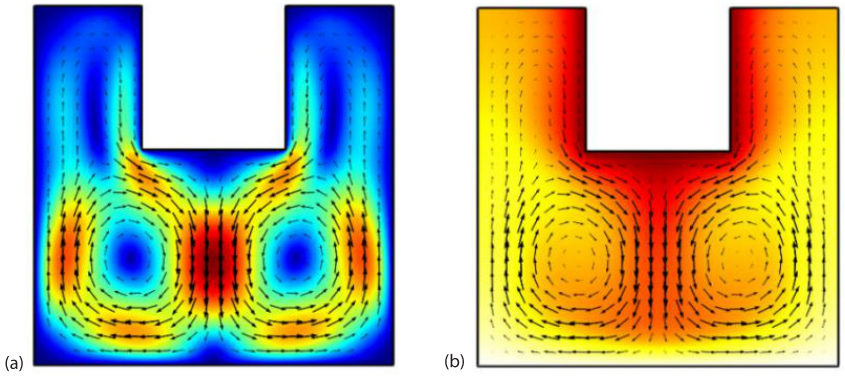

Figure 6. The velocity vectors with (a) velocity magnitude and (b) isosurface with m = 3, $H_C = L_C = 0.4$. Ra = 10^5, and $\phi_{hp} = 0.05$

Figure 7(a) shows the variation of $\overline{Nu}$ for different Rayleigh number with different cold rib dimension at m = 3 and $\phi_{hp} = 0.05$. As Rayleigh number increases, the value of $\overline{Nu}$ increases except for $L_C = H_C = 0.9$, where they are about equal. Considering that the enclosure becomes too narrow for heat convection occur, this situation produces almost parallel

isotherms for all Rayleigh number. It also noted that for Ra = 10^5, the value of $\overline{\text{Nu}}$ for $L_C = H_C = 0.7$ is lower than $L_C = H_C = 0.6$, before increasing again for $L_C = H_C \geq 0.8$. This is because at the specific cold rib dimension, the enclosure space at the left and right are small enough for the fluid to form four Rayleigh-Benard cells, which lower the value of $\overline{\text{Nu}}$. For $L_C = H_C \geq 0.8$, the enclosure space is too small to produce four cells, so only two cells are formed, and causes $\overline{\text{Nu}}$ to increase. For Ra = 10^6, the value of $\overline{\text{Nu}}$ decreases for $L_C = H_C \geq 0.7$ due to the smaller enclosure space for the fluid to undergo heat convection. This result is in agreement with the isotherm lines in fig. 5. Figure 7(b) presents the variation of $\overline{\text{Nu}}$ for different Rayleigh numbers with different nanoparticle shapes at $L_C = H_C = 0.4$ and $\phi_{hp} = 0.05$. From fig. 7(b), the value of $\overline{\text{Nu}}$ increases as Rayleigh number increases with sphere ($m = 3$) being the lowest and blade ($m = 8.6$) being the highest. As the empirical nanoparticle shape factor m increase, the total surface area of the nanoparticle increases [16]. This causes more heat can be dissipated and in turns, produces a higher heat transfer rate. From fig. 7(b), the increase of $\overline{\text{Nu}}$ for Ra = 10^6 is the highest for increasing m. At higher Rayleigh number, turbulent flows agitate the nanofluid and force the nanoparticles to transfer heat faster.

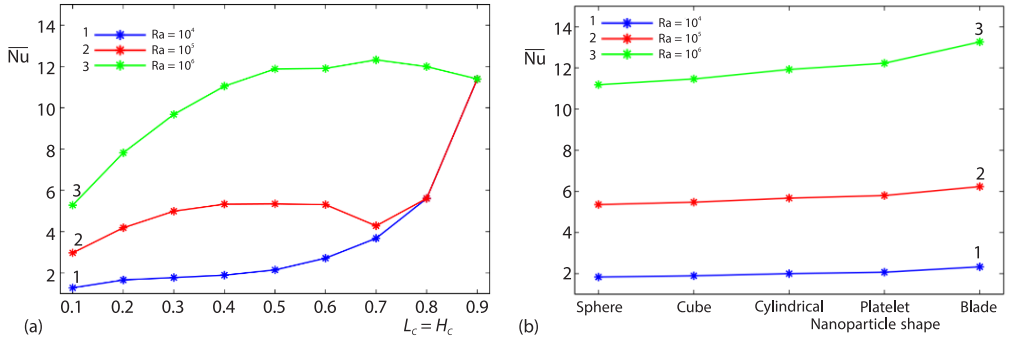

Figure 7. The variation of $\overline{\text{Nu}}$ for different Rayleigh numbers with: (a) different cold rib dimensions at $m = 3$ and $\phi_{hp} = 0.05$ and (b) different nanoparticle shapes at $H_C = L_C = 0.4$, and $\phi_{hp} = 0.05$

Figure 8 presents the variation of local Nusselt numbers, Nu_{loc}, at the hot wall with different cold rib dimension at $m = 3$ and $\phi_{hp} = 0.05$ for Ra = 10^5 and Ra = 10^6. From fig. 8, the highest Nu_{loc} is at $x = 0.5$ for all Rayleigh numbers. The reason is that distance between the hot wall and the cold rib is the shortest at that position and the fluid-flow at all cases forces the cold fluid to flow

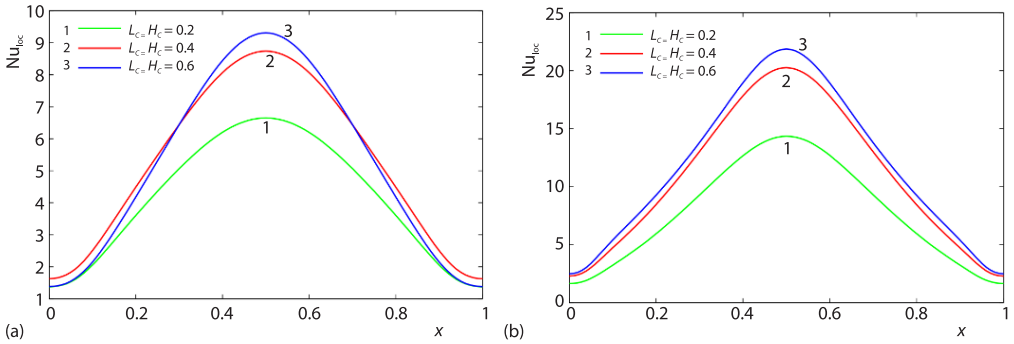

Figure 8. The variation of Nu_{loc} at the hot wall with different cold rib dimensions at $m = 3$ and $\phi_{hp} = 0.05$ for: (a) Ra = 10^5 and (b) Ra = 10^6

into the direction of the hot wall at $x = 0.5$. In both figures, the graphs are symmetric due to the symmetric characteristics of the enclosure. It is also noted that as the cold rib dimension increases, the value of Nu_{loc} also decreases for both $Ra = 10^5$ and $Ra = 10^6$. The gradient of the Nu_{loc} for $Ra = 10^5$ is lower than $Ra = 10^6$ due to the presence of turbulent flow when $Ra = 10^6$. This makes the fluid-flow moves faster at the center of each Rayleigh-Benard cells when $Ra = 10^6$ than $Ra = 10^5$. In addition, the heat transfer of the fluid is more concentrated at the middle of the hot wall when $Ra = 10^6$ than $Ra = 10^5$.

Figures 9(a) and 9(b) present the Nu_{loc} with different nanoparticle shapes at $Ra = 10^6$ and $\phi_{hp} = 0.05$ for hot wall and cold wall, respectively. From fig. 9(a), the maximum Nu_{loc} occurred at the middle of the hot wall for blade nanoparticle shape. The higher the empirical nanoparticle shape factor, m, the greater the nanoparticle surface area [16]. This means the greater surface area is in contact with the fluid, which enhance the heat transfer inside the enclosure. For fig. 9(b), the value of Nu_{loc} increases before dropping until it reaches the corner G for all nanoparticle shapes. The same behaviour can be said for side EF. This situation occurs because the two corners F and G restrict the fluid-flow between the narrower upper part and the wider lower part of the enclosure. This change of width causes the fluid-flow to rush to the middle-lower part of the enclosure, and in turns, produces a relatively higher velocity at the vicinity of the corners F and G. Since the turbulent flows dominate at $Ra = 10^6$, the fluid-flow around this region increases rapidly. This causes the heat from bottom to be in contact with the cold wall, specifically at the F and G corners. Both corners possess higher fluid velocity and dissipate heat at a higher rate compared to other corners.

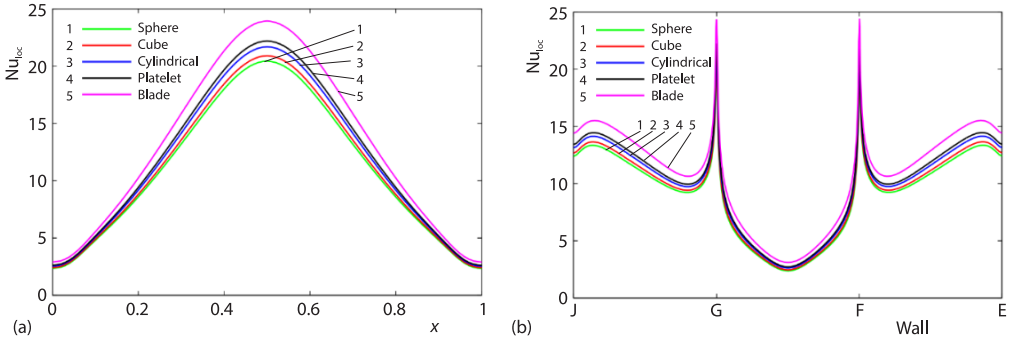

Figure 9. The variation of Nu_{loc} with different nanoparticle shape at $Ra = 10^6$ and $\phi_{hp} = 0.05$ for: (a) hot wall and (b) cold wall

Conclusions

In this paper, the effect of the nanoparticle shapes on the natural-convection heat transfer of Cu-Al_2O_3-water hybrid nanofluid inside a *U*-shaped enclosure is presented. The conclusions that can be drawn from the work are as follows.

- Addition of metallic nanoparticles to metallic oxides nanofluid increases the heat transfer rate inside enclosures.
- An increase in the cold rib dimension increases the rate of heat transfer, except when $L_C = H_C = 0.7$ for $Ra = 10^5$ and $L_C = H_C \geq 0.7$ for $Ra = 10^6$.
- The highest $\overline{Nu}$ occurs when using blade nanoparticle shape ($m = 8.6$) while sphere ($m = 3$) is the lowest for all Rayleigh numbers.

These results obtained can be used in many applications in industries such as car radiators and nuclear reactor [20]. It is hoped that this investigation can be expanded to include turbulent fluid-flow and non-uniform thermal profile.

Acknowledgment

The authors would like to acknowledge the Ministry of Higher Education Malaysia and the University of Malaya for the financial support through the Faculty Research Grant GP-F004H-2018 and Impact Oriented Interdisciplinary Research Grant IIRG006C-19IISS.

Nomenclature

C_p – specific heat capacity, [J°C^{-1}kg^{-1}]
g – gravitational acceleration, [ms^{-2}]
H_C – cold rib height, [m]
k – thermal conductivity, [Wm^{-1}K^{-1}]
L_C – cold rib length, [m]
$\underline{m}$ – nanoparticle shape factor, [–]
$\overline{\text{Nu}}$ – average Nusselt number, [–]
Nu_{loc} – local Nusselt number, [–]
P – dimensionless pressure, [–]
p – pressure, [Pa]
Pr – Prandtl number [–]
Ra – Rayleigh number [–]
T – temperature, [°C]
U, V – dimensionless velocity in x- and y-axis, [–]
u, v – velocity in x- and y-axis, [ms^{-1}]
W – enclosure length and width, [m]
x, y – Cartesian co-ordinates, [–]
X, Y – dimensionless Cartesian co-ordinates, [–]

Greek symbols

α – thermal diffusivity, [m^{2}s^{-1}]
β – thermal expansion coefficient, [K^{-1}]
θ – dimensionless temperature, [–]
μ – dynamic viscosity, [kgm^{-1}s^{-1}]
ν – kinematic viscosity, [m^{2}s^{-1}]
ρ – fluid density, [kgm^{-3}]
ϕ – nanoparticle volume fraction, [–]
ψ – stream function, [–]

Subscripts

bf – base fluid
C – cold wall
H – hot wall
hnf – hybrid nanofluid
hp – hybrid nanoparticle

References

[1] Cho, C.-C., *et al*., Enhancement of Natural-Convection Heat Transfer in A U-Shaped Cavity Filled with Al_2O_3-Water Nanofluid, *Thermal Science*, *16* (2012), 5, pp. 1317-1323
[2] Ghasemi, B., Magnetohydrodynamic Natural Concection of Nanofluids in U-Shaped Enclosures, Numerical Heat Transfer, Part A: Applications: *An International Journal of Computation and Methodology*, *63* (2013), 6, pp. 473-487
[3] Mohebbi, R., *et al*., Heat Source Location And Natural-convection in A C-Shaped Enclosure Saturated by A Nanofluid, *Physics of Fluids*, *29* (2017), 122009
[4] Ma, Y., *et al*., Effect of Hot Obstacle Position on Natural-Convection Heat Transfer of MWCNT-Water Nanofluid in U-Shaped Encosure Using Lattice Boltzmann Method, *International Journal of Numerical Methods for Heat & Fluid-Flow*, *29* (2019), 1, pp. 223-250
[5] Ali, H. M., *et al.*, Heat Transfer Enhancement of Car Radiator Using Aqua Based Magnesium Oxide Nanofluids, *Thermal Science*, *19* (2015), 6, pp. 2039-2048
[6] Kilic, M., Ali, H. M., Numerical Investigation of Combined Effect of Nanofluids and Multiple Impinging Jets on Heat Transfer, *Thermal Science*, *23* (2019), 5B, pp. 3165-3173
[7] Ashorynejad, H. R., Shahriari, A., The MHD Natural-Convection of Hybrid Nanofluid in An Open Wavy Cavity, *Results in Physics*, *9* (2018), June, pp. 440-455
[8] Hayat, T., Nadeem, S., Heat Transfer Enhancement with Ag-CuO-Water Hybrid Nanofluid, *Results in Physics*, *7* (2017), June, pp. 2317-2324
[9] Tayebi, T., Oztop, H. F., Entropy Production During Natural-Convection of Hybrid Nanofluid in An Annular Passage between Horizontal Confocal Elliptic Cylinders, *International Journal of Mechanical Sciences*, *171* (2020), 105378
[10] Tayebi, T., *et al*., Natural-Convection and Entropy Production in Hybrid Nanofluid Filled-Annular Elliptical Cavity With Internal Heat Generation And Absorption, *Thermal Science And Engineering Progress*, *19* (2020), 100605

[11] Al-Srayyih, B. M., *et al*., Natural-Convection Flow of A Hybrid Nanofluid in A Square Enclosure Partially Filled with a Porous Medium Using A Thermal Non-Equilibrium Model, *Physics of Fluids*, *31* (2019), 043609
[12] Tayebi, T., Chamkha, A. J., Magnetohydrodynamic Natural-convection Heat Transfer of Hybrid Nanofluid in a Square Enclosure in the Presence of a Wavy Circular Conductive Cylinder, *Journal of Thermal Science and Engineering Applications*, *12* (2020), 3, 031009
[13] Snoussi, L., *et al*., Natural-Convection Heat Transfer in a Nanofluid Filled U-Shaped Enclosures: Numerical Investigations, *Heat Transfer Engineering*, *39* (2018), 16, pp. 1450-1460
[14] Brinkman, H. C., The Viscosity of Concentrated Suspensions and Solutions, *The Journal of Chemical Physics*, *20* (1952), 4, 571
[15] Hamilton, R. L., Crosser, O. K., Thermal Conductivity of Heterogenous Two-Component Systems, *Industrial & Engineering Chemistry Fundamentals*, *1* (1962), 3, pp. 187-191
[16] Timofeeva, E. V., *et al*., Particle Shape Effects on Thermophysical Properties of Alumina Nanofluids, *Journal of Applied Physics*, *106* (2009), 014304
[17] Bhati, M. A., *Fundamental Finite Element Analysis and Applications*: *with Mathematica and Matlab Computations*, John Wiley & Sons, New Jersey, N. Y., USA, 2005
[18] Buchanan, A. M., Fitzgibbon, A. W., Damped Newton Algorithms for Matrix Factorization with Missing Data, *Proceedings*, 2005 IEEE Computer Society Conference on Computer Vision and Pattern Recognition (CVPR'05), San Diego, Cal., USA, 2005, pp. 316-322
[19] Mliki, B., *et al*., Lattice-Boltzmann Analysis of MHD Natural-Convection of CuO-Water Nanofluid in Inclined C-Shaped Enclosures under the Effect of Nanoparticle Brownian Motion, *Powder Technology*, *308* (2017), 16 pp. 70-83
[20] Yu, W., Xie, H., A Review on Nanofluids: Preparation, Stability Mechanisms And Applications, *Journal of Nanomaterials*, *2012* (2012), 435873

Paper submitted: August 18, 2020
Paper revised: October 19, 2020
Paper accepted: January 9, 2021